International Journal of High-Rise Buildings
December 2019, Vol 8, No 4, 255-264
https://doi.org/10.21022/IJHRB.2019.8.4.255

International Journal of
High-Rise Buildings
www.ctbuh-korea.org/ijhrb/index.php

Numerical Simulation of Wind Pressures on a High-rise Building by Auto-mesh System

Yuanzhe Tang[1] and Shuyang Cao[2†]

[1]*College of Civil Engineering, Tongji University, Shanghai 200092, China*
[2]*State Key Laboratory for Disaster Reduction in Civil Engineering, Tongji University, Shanghai 200092, China*

Abstract

This paper describes large eddy simulation of wind pressures on a square cylinder in a uniform flow and a high-rise building immersed in an atmospheric turbulent boundary layer. For the atmospheric boundary layer case, the inflow turbulence is generated by a numerical wind tunnel. In the numerical simulation, particular attention is devoted to the performance of an auto hexahedral non-structural mesh. Both simulations are performed for three grid systems: an auto hexahedral non-structured grid, a structured Cartesian grid and a non-structured triangular prism grid, and for three grid numbers. The present study shows that the auto hexahedral unstructured mesh achieves the best simulation results for wind pressures on the square cylinder and the high-rise building. When the grid number is sufficiently large, the differences among the results obtained from the three investigated grid systems are not significant. However, the advantage of the auto hexahedral unstructured mesh becomes clear when the grid number decreases, because it enables a balanced distribution of orthogonal grids. The results described in this paper demonstrate that the auto hexahedral non-structured mesh has good potential applicability to simulation of urban flows.

Keywords: Wind pressure; Large eddy simulation; Auto mesh; High-rise buildings; Inflow turbulence.

1. Introduction

Over the past several decades, CFD-based numerical simulation has undergone a successful transition from an emerging field into an increasingly established field in wind engineering research, practice and education. After the Dutch standard (Blocken, 2013) accepted CFD as a tool for evaluating pedestrian-level wind conditions and wind comfort in urban areas, the Architectural Institute of Japan (AIJ) recommended it as an alternative tool for determining wind loads on buildings (2015). The decision to treat wind tunnel experimentation and CFD as equals in standards/recommendations has encouraged, and will definitely continue to encourage, the use of CFD for evaluating wind forces on buildings in urban areas. This is particularly important because of the necessity to analyze extensive urban areas, which is difficult to achieve with wind tunnel experiments. However, as emphasized by Blocken (2013), acceptance of CFD does not absolve the user from providing quality assurance. The CFD user needs to pay more attention to the accuracy, stability and efficiency of the simulation than before because the simulation results may be directly utilized in structural design.

A lot of numerical simulations have been performed to calculate wind pressures acting on high-rise buildings. Ono et al (2001) carried out large eddy simulation of wind pressures on buildings in a real urban area, in which all building surfaces had to be adjusted to be parallel or perpendicular to the adopted Cartesian grid. Tamura et al (2003) performed large eddy simulation of wind loads on tall buildings in an urban area, in which the building shape was modeled by an immersed boundary method. Nozu et al (2008) utilized geographic information system (GIS) data and a nested grid technique to simulate Tokyo's strong wind field, and showed that the multi-layer nested grid system was better than other grid systems for simulating an urban flow field. Huang et al (2008) explored an effective method for evaluating wind effects on tall buildings and found that LES with a dynamic subgrid-scale (SGS) model could give satisfactory predictions of mean and fluctuating wind loads on tall buildings. Recently, Phillips and Soligo (2019) discussed the development trend of CFD for building wind simulations. These previous studies have shown that one practical difficulty in simulating the wind load on buildings in an urban area, among many others, is the grid generation technique for modeling complicated building shapes, and this problem worsens with increase in city area and building numbers. Developing a mesh system with high quality, fast generation speed and high precision is a crucial issue in CFD studies of real urban areas.

Many other factors also affect the effectiveness of CFD simulation, among which the grid system has a great influence on the stability of numerical simulation and the accuracy of the final results. A reasonable grid system

†Corresponding author: Shuyang Cao
Tel: 86-21-65981318 ; Fax: 86-21-65986507
E-mail: shuyang@tongji.edu.cn

helps to produce satisfactory results without the need for too many computational resources. However, an insufficient number of grids or poor mesh quality may even make the calculation diverge. Different grid types, e.g., structured or unstructured, also have a great impact on the final results. The structured grid can produce spatial modal solutions with good equilibrium accuracy over a wide range from low order to high order, and thus improve accuracy. However, resolution of the solution of an unstructured grid is not uniform, so the accuracy is decreased and the computational efficiency is lower than that of the structured grid. Frohlich et al (1998) carried out large eddy simulation of flow around a cylinder with a structured and an unstructured grid, from which the variation of simulation accuracy with grid type was studied. Cao and Tamura (2016) compared simulation results for a square cylinder for a Reynolds number of 22000 of structured and triangular unstructured grids, and tried to identify the influence of grid type on the simulation of vortex shedding and resulting aerodynamic forces. Weatherill (1990) discussed the performance of structured-unstructured hybrid grids and verified its advantages through designed numerical experiments. Although the mesh generation of an unstructured grid system is relatively complex, it has good shape adaptability and is very effective for mesh generation in some computational domains with complex shapes or boundary shapes, which is difficult to achieve with a structured grid. In addition to utilizing the structured-unstructured hybrid grid technique to meet the requirements of resolving building shape, the automatic grid generation method is suitable if a large area with many buildings needs to be discretized. Through an automatic grid generation algorithm, the grid system can be formed quickly in the domain, and the grid quality can be guaranteed by pre-set requirements. Uemura and Saito (1993) proposed an automatic grid generation algorithm for tetrahedral unstructured grids, in which a grid system with a small number of rough meshes is generated in the computational domain first, followed by recursive local refinement until all meshes meet the size distribution requirements. They also investigated the feasibility of this algorithm in simulating the wind field around a three-dimensional building.

The present study investigates the performance of an automatic hexahedral unstructured grid system in simulating wind pressures on a high-rise building immersed in an atmospheric boundary layer. Two other kinds of widely utilized grid systems, i.e., the structured Cartesian grid and the unstructured triangular prism grid, are utilized for comparison. In addition, simulation of flow around a square cylinder in uniform flow is also performed in order to enhance understanding of the performance of an automatic hexahedral unstructured grid, because more experimental and CFD data are available for the case of a square cylinder. Furthermore, LES simulations with three grid systems for both the square cylinder and the high-rise building cases are carried out with three grid numbers to check the dependence of grid performance on grid number. The simulation results obtained for different grid systems and different grid numbers are compared with each other, and also with experimental data, and the performances of the automatic hexahedral unstructured grid system as well as its applicability to numerical simulation of wind load on buildings in urban areas are discussed.

2. Numerical simulation details

2.1. HEX auto-mesh system

We utilized the auto-mesh software HEXPRESS, which is a sub-software of CFD software NUMECA, developed by the European space agency (ESA), to generate HEX

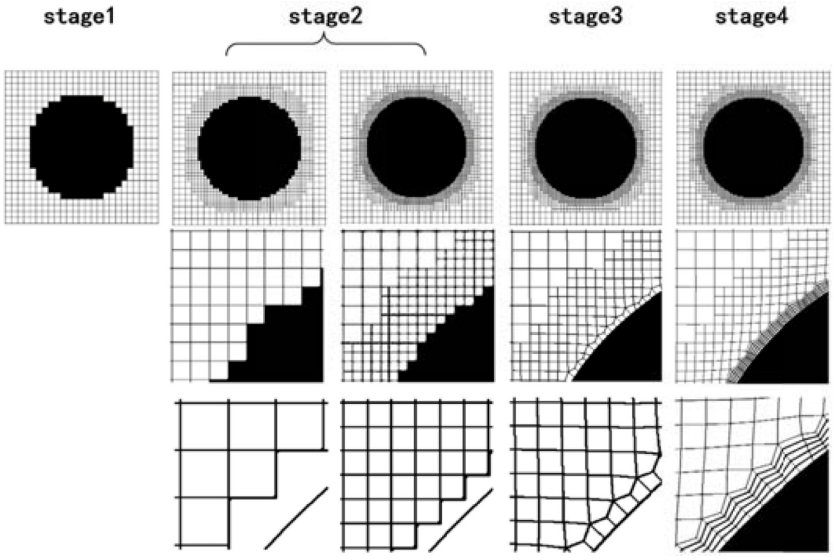


Figure 1. Generation procedure of HEX grid.

grids. The basic concept of this auto-mesh technique is fast generation of hexahedron or hexahedron-based unstructured grids for any geometry. The hexahedral unstructured mesh automatic generation method is based on the octree (3D) principle for subdividing the spatial mesh until it meets the requirements of mesh resolution. Figure 1 illustrates the general process of mesh generation for a sphere. In stage 1, an initial grid system is established in the domain with a relatively large mesh, and the inner part of the sphere and the grid intersecting with the sphere wall surface are deleted. In stage 2, the mesh around the sphere is refined by shortening the mesh size by halving it each time. The coarsely meshed grids are subdivided continuously, i.e., the cuboid meshes in 3d are subdivided into eight small cuboids until the mesh size meets the requirements. In stage 3, the mesh near the wall surface is repaired and deformed to make the mesh adhere to the sphere surface. In stage 4, the first several layers of the surface grids are segmented to generate a number of layers orthogonal to the sphere surface. At the same time, some outer grids are adjusted to make them transition with the wall grid. This procedure makes the mesh around the target gradually refine and deform to fit the target surface.

Because the generated unstructured hexahedral grid is arranged in a Cartesian coordinate system, it is easy to split and reconstruct it. Therefore, it is beneficial to adopt an adaptive grid technology to refine the grid along some large gradient of speed or pressure area, and to arrange fewer grids in places with small gradients. Thus, the accuracy of complex flow field simulation can be guaranteed while the total number of meshes is reduced. Due to the characteristics of the grid generation procedure, the generated grid is basically rectangular in space, and its quality is very high. To overcome the problem of viscosity, the grid of the first layer of the wall surface is divided to meet the requirements of grid thickness. In short, this auto mesh technique has the advantages of both structured and unstructured grids.

2.2. Numerical simulation outlines

Time-dependent unsteady finite volume approximation is carried out to reproduce the wind flow and wind pressures acting on buildings. The governing equations for the three-dimensional incompressible large-eddy simulation are the filtered continuity equation and the Navier-Stokes equation expressed as:

$$\frac{\partial \bar{u}_i}{\partial x_i} = 0 \tag{1}$$

$$\frac{\partial \bar{u}_i}{\partial t} + \frac{\partial}{\partial x_j}(\bar{u}_i \bar{u}_j) = -\frac{1}{\rho}\frac{\partial \bar{p}}{\partial x_i} + \frac{1}{\rho}\frac{\partial}{\partial x_j}\left(\mu \frac{\partial \bar{u}_i}{\partial x_j}\right) - \frac{1}{\rho}\frac{\partial \tau_{ij}}{\partial x_j} \tag{2}$$

where $\bar{u}_i$ (i = 1, 2, 3) and $\bar{p}$ are the three filtered velocity components and pressure, respectively, ρ is the air density, and τ_{ij} is the SGS stress. The principal idea of LES is to directly resolve the grid scale turbulence while modeling the sub-grid-scale turbulence via low-pass filtering of the governing equations of fluids. SGS stress can be modeled as:

$$\tau_{ij} = \frac{1}{3}\delta_{ij}\tau_{kk} - 2\nu_e \bar{S}_{ij}, \quad \bar{S}_{ij} = \frac{1}{2}\left(\frac{\partial \bar{u}_i}{\partial x_j} + \frac{\partial \bar{u}_j}{\partial x_i}\right) \tag{3}$$

where ν_e is the subgrid-scale turbulent viscosity, $\bar{S}_{ij}$ is the rate-of-strain tensor for the resolved scale, and δ_{ij} is the Kronecker delta. The standard Smagorinsky model is used to calculate turbulence viscosity.

The open source solver OpenFOAM is used to solve the governing equations, and the options offered by OpenFOAM for simulation are carefully selected in order to achieve reliable results. The second-order LUST divergence scheme, which is a fixed blended scheme with 0.25 linear upwind and 0.75 linear weights, is used for the convection term. The PIMPLE algorithm is used to solve the discretized equations, in which governing equations are solved sequentially because of their non-linearity and coupling characteristics, and the solution loop is carried out iteratively in order to obtain a converged numerical solution. The pressure field is extracted by solving a pressure correction equation obtained by manipulating continuity and momentum equations, while the velocity field is obtained from the momentum equations. In addition, the convergence criteria of the iterative calculation are set to 1×10^{-5} for both velocity and pressure. Meanwhile, an implicit second-order time-advancement scheme is chosen for temporal discretization to obtain stable and accurate simulation.

3. Simulation of wind pressure on a square cylinder in uniform Flow

Numerical experiment setting and numerical details

In order to investigate the basic performance of the HEX grid, numerical experiments are first carried out by performing a series of simulations of wind pressures on a square cylinder at Re = 22000. A lot of experimental and numerical studies have been carried out on flow around a square cylinder at Re = 22000, so a lot of data can be utilized for validation. Figure 2 illustrates the computational domain, which is $28D \times 24D \times 4D$ (D: side length of square cylinder). The blockage ratio is about 8%. Simulations

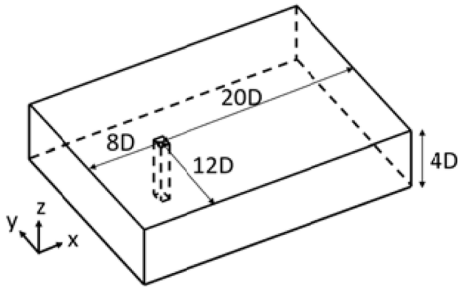


Figure 2. Computational domain.

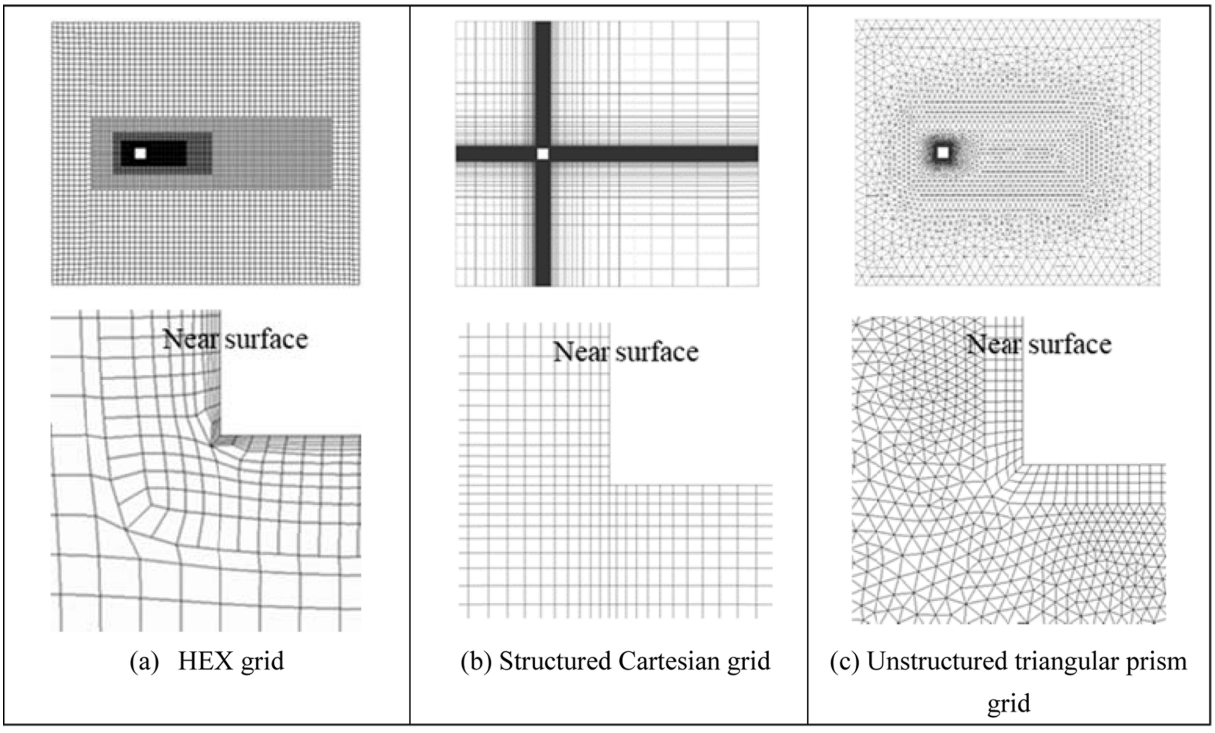


Figure 3. Examples of grid systems for grid number of 1.4 million. (*x*-*y* plan)

are performed under three grid systems, i.e., the HEX grid, structured Cartesian grid and unstructured triangular prism grid, with three grid numbers, i.e., 0.45 million, 1.4 million and 4.8 million, respectively. For example, Figure 3 shows the *x*-*y* plan of three grid systems at a grid number of 1.4 million. All grid systems are closely spaced near the body surface, with the grid closest to the cylinder surface possessing $0.1\sqrt{\mathrm{Re}}$ ($y^+ \approx 1$) to capture the behavior of the separated shear layer. The auto-split of the cuboid grid continues until the mesh size decreases to four times the size of the finest grid near the body, which is decided explicitly. It can be realized that, when the total grid number and finest grid size near the cylinder are fixed, the structured Cartesian grid inevitably has a very large side ratio in the belt-like area near the center of the computational domain. Conversely, the HEX grid is well distributed over the whole domain and remains orthogonal. In addition, there are 80 grids in the span-wise *z* direction, which are the same for all simulation cases.

The boundary conditions are as follows. Uniform flow with velocity $U = 1$ at the inlet boundary and convective boundary conditions at the outlet boundaries. Symmetric boundary conditions are applied at the lateral, top and bottom boundaries. A no-slip boundary condition is imposed on the cylinder surface. The zero-gradient pressure boundary condition is applied at the inlet boundary and the cylinder surface. Fixed pressure value 0 is applied at the outlet boundary. The simulation starts from rest. The flow field analysis is conducted with respect to 30 vortex shedding cycles after vortex shedding becomes stable.

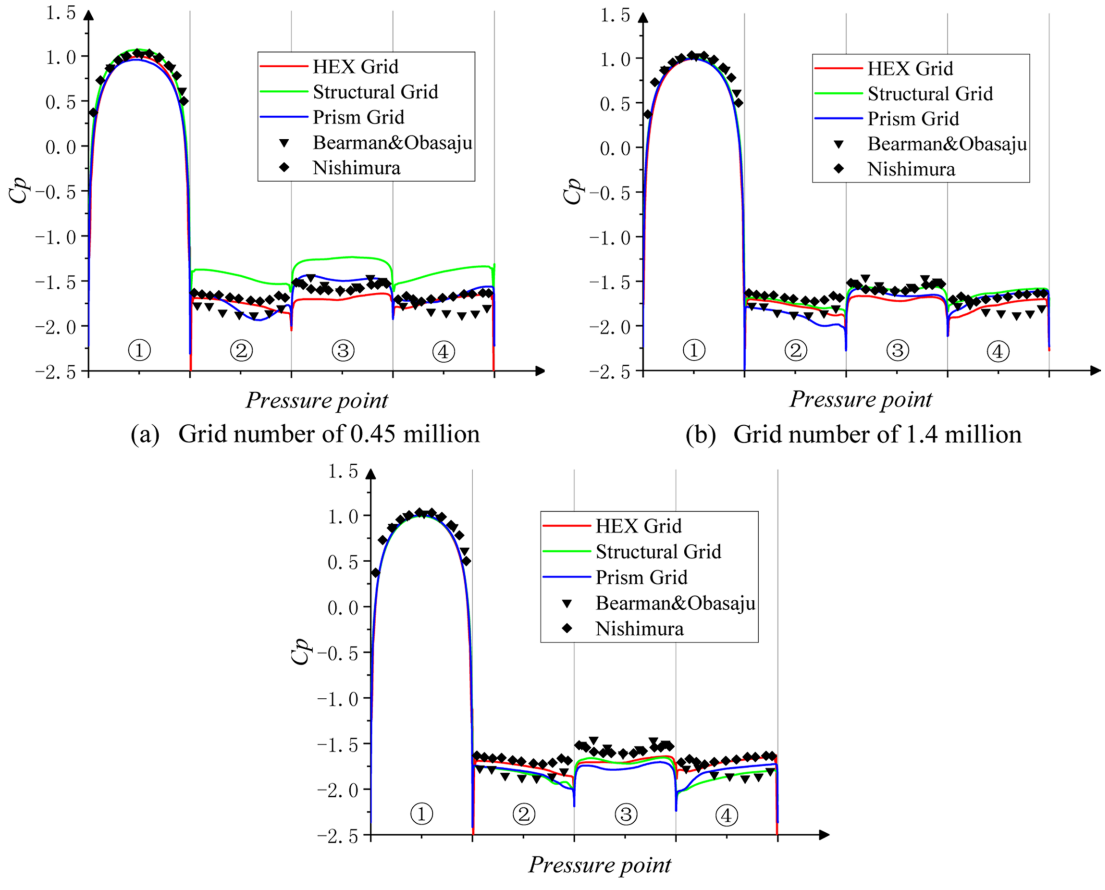
3.2. Results and discussions

Table 1 summarizes the integral parameters of flow around a square cylinder obtained in the present study, i.e. mean drag coefficient, root mean squares of drag and lift coefficients, Strouhal number and wake recirculation length obtained for three grid systems, each with three grid numbers, and compares them with experimental data (Cheng et al. 1992, McLean and Gartshore 1992, Lyn et al 2006, Norberg 1993, Lee 2006, Durao et al. 1988) and numerical simulation results (Lubcke et al. 2001, Srinivas et al. 2006). The numerical procedure, boundary conditions, initial conditions, computational domain and finest grid size near the body do not change with grid type. Thus, the differences in integral parameters shown in Table 1 for a certain grid number are considered to result mainly from the grid type. Table 1 shows that the HEX, structured and non-structured grids produce almost the same results for a grid number of 4.0 million, the deviations of which are within the deviation range between the experimental and numerical results obtained by other researchers. However, when the total grid number decreases, the three different grid systems produce different results, especially when the grid number is only 0.45 million. Note that the values of integral parameters change significantly when the number of structural Cartesian grid changes from 1.40 million to 0.45 million, while the results of HEX for a grid number of 0.45 million are still acceptable. These results imply that the HEX grid system performs the best among the three investigated grid systems.

Table 1. Comparisons of integral parameters of square cylinder in uniform flow

Grid No. (million)	Grid type	C_d-mean	C_d-rms	C_l-rms	S_t	l_r / D
0.45	HEX	2.18	0.207	1.39	0.134	1.16
	Structure	1.76	0.363	0.77	0.14	1.36
	Non structured prism	2.07	0.272	1.27	0.123	1.09
1.40	HEX	2.26	0.161	1.15	0.128	1.16
	Structure	2.20	0.261	1.24	0.129	1.27
	Non structured prism	2.30	0.239	1.52	0.131	1.07
4.0	HEX	2.24	0.187	1.22	0.124	1.13
	Structure	2.28	0.247	1.51	0.131	1.14
	Non structured prism	2.34	0.214	1.64	0.131	1.08
Lubcke et al (2001)		2.18	-	1.47	0.130	1.06
Srinivas et al (2006)		2.14	0.17	1.12	0.135	1.31
Cheng et al (1992)		1.9-2.1	0.1-0.2	0.1-0.6	-	-
McLean et al (1992)		1.9-2.1	0.1-0.2	0.7-1.4		
Lyn et al (2006)		2.10	-	-	0.132	1.38
Norberg (1993)		2.10	-	-	0.130	1.37
Lee (2006)		2.05	0.23	-	0.122	-
Durao et al (1988)		-	-	-	0.138	1.33

Figure 4 plots the distribution of mean pressure coefficient C_p around the square cylinder in comparison with the experimental data of Bearman and Obasaju (1982) and Nishimura and Taniike (2000). The mean pressure coefficient C_p is defined as $C_p=\frac{p-p_\infty}{0.5\rho U^2}$, in which



(a) Grid number of 0.45 million

(b) Grid number of 1.4 million

(c) Grid number of 4.8 million

Figure 4. Distribution of mean pressure coefficient around square cylinder.



(a) HEX grid (b) Structure Cartesian grid (c) Unstructured triangular prism grid

Figure 5. Comparison of iso-vorticity surface of instantaneous flow field. (grid number is 4 million) (wz = ±3)

p is the pressure acting on the body surface, p_∞ is the reference pressure, and U is the mean velocity of oncoming flow. The X coordinate of Figure 4 denotes one circle around the square cylinder. The windward side, two crosswind sides, and leeward side are marked 1, 2, 3 and 4. Figure 4c shows that all three grid systems simulate the wind pressure distribution well when the grid number is 4.0 million. However, with decrease in grid number, the results deviate. For instance, the results for the structured grid clearly deviate from those of the other two grids and the experiments when the grid number is 0.45 million.

Obvious differences resulting from the grid system can be found in Figure 5, which compares the iso-vorticity surface of the instantaneous flow field when the grid number is 4.0 million, at which the integral parameter even matches with each other. An abundant vortex structure is exhibited in Figure 5a for the HEX grid. However, the structured Cartesian grid does not capture the wake flow due to the too coarse grids in the wake region, as shown in Figure 5b. Also, Figure 5c shows that the wake flow of the unstructured triangular prism grid loses its fine vortex structures. The well balanced Cartesian HEX grid is considered to have contributed to this result.

4. Simulation of wind pressure on a high-rise building in ABL

4.1. Simulation of inflow turbulence

Figure 6 illustrates the computation setting for simulating the flow around a high-rise building immersed in an atmospheric boundary layer. The left side of Figure 6 shows a numerical wind tunnel designed to simulate the inflow turbulence, which is then imposed at the inflow boundary of the simulation of flow around the high-rise building shown on the right side at each time step. The high-rise building model 0.1008 m long, 0.0357 m wide and 0.21 m high is located at the center of the computational domain 3.15 m long, 2.5 m wide and 2.1 m high. The settings of model and computational domain sizes are designed to match the boundary layer wind tunnel experiment, whose test data are utilized for comparison in the present study (Noda 2016). The blocking rate is less than 1%. Only one flow direction is considered in this study: that in which the wind blows against the short side of the building model. The Reynolds number Re = 140000.

A category C oncoming flow as specified by AIJ recommendation (AIJ, 2015) is generated in a numerical wind tunnel. The simulated oncoming boundary layer is required to have similar wind characteristics to the experiment (Noda 2016), i.e., oncoming boundary layer height 1.125 m, mean velocity at building height 10m/s, and power law index of mean velocity profile $\alpha = 0.2$. In order to reproduce these wind speed characteristics, four spires and three kinds of rough elements with different heights are placed as passive devices on the floor of the computational domain to enhance the development of turbulence. The height and breadth at the bottom of the spire are 1.42 m and 0.183 m, following the suggestion given by Irwin (1981). The biggest roughness elements are 0.142 m high, 0.071 m long and 0.0355 m wide. The along-wind and cross-wind distances of the roughness elements is 0.71 m and 0.355 m, respectively.

A hybrid grid system is adopted to discretize the computational domain. As shown in Figure 7, a large tetrahedral mesh is used in the upper half domain of the wind tunnel. The tetrahedral grid is adopted around the thin spire because it has good adaptability. The triangular prism grid is used around the roughness elements, while the standard structured

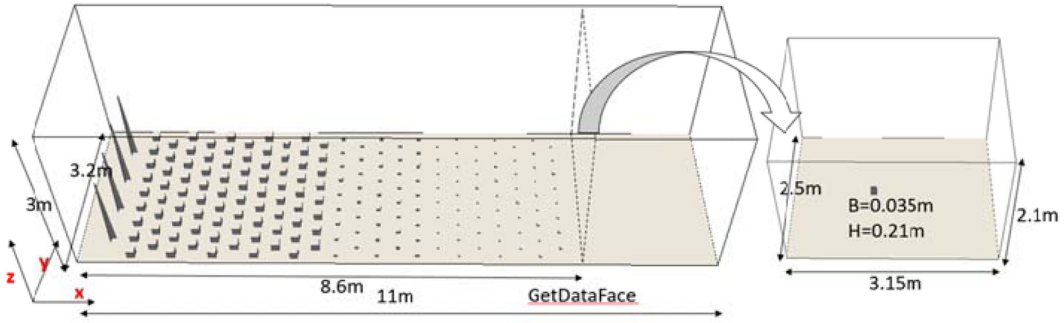


Figure 6. Computation setting for simulating flow around high-rise building.

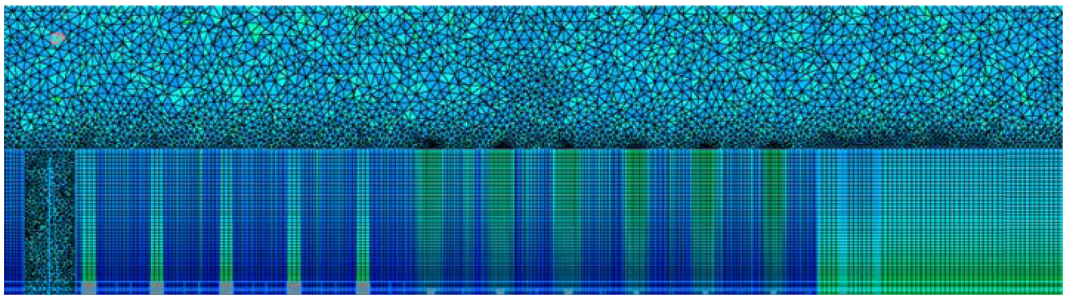


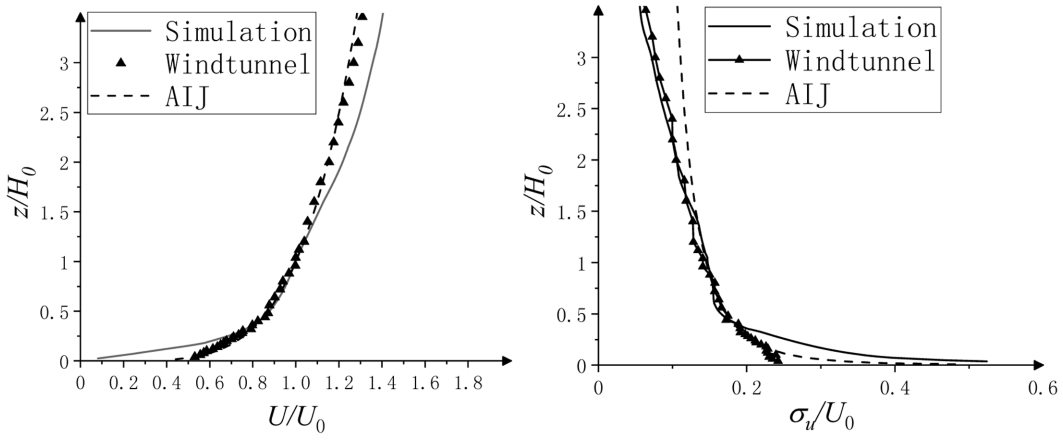
Figure 7. Grid system of numerical wind tunnel.

grid is used in the wake area behind the rough elements. The total grid number of this numerical wind tunnel is 5.6 million.

The generated flow field is utilized as the inflow data for the simulation of wind pressures on the high-rise building after interpolation. Figures 8a and 8b compare the vertical profiles of mean velocity and turbulence intensity obtained by numerical simulation with the experimental data and AIJ recommendations. The x and y coordinates are normalized by the wind speed at the boundary layer height and building height, respectively. The vertical profiles of mean velocity and turbulence intensity agree closely with both the experiment and AIJ recommendations within the building height except for the lower heights near the ground. Figure 8c illustrates the power spectrum of wind speed fluctuation at building height, which agree with the Karman type except for the high frequency range.

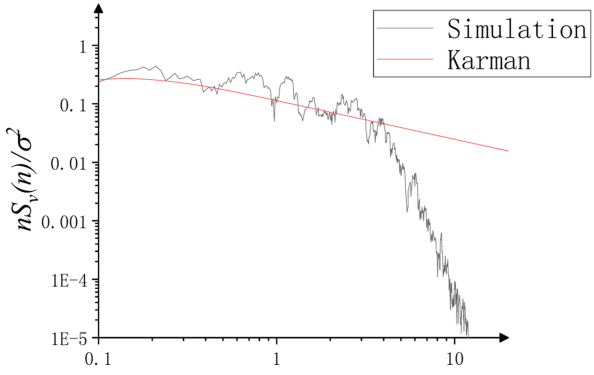
4.2. Numerical experiment setting numerical details

The performance of HEX grid in simulating wind



(a) Mean wind speed

(b) Turbulent intensity



(c) Power spectrum of wind speed fluctuation at building height

Figure 8. Comparison of profiles of mean velocity and turbulence intensity.

pressures acting on a high-rise building is further studied. The simulations adopt a HEX grid, a structured Cartesian grid and an unstructured triangular prism grid, and consider three grid numbers: 1.8 million, 3 million and 7.2 million, respectively. Figure 9 illustrates the grid systems when the grid number is 1.8 million as an example. As in previous calculations, all grid systems are closely spaced near the body surface ($y^+ \approx 5.0$) for the grid closest to the building surface) to capture the behavior of the separated shear layer, and $y^+ \approx 10$ is adopted for the grid closest to the ground surface to resolve the boundary layer. The auto-split of the cuboid grid continues until the mesh size decreases to four times the size of the grid closest to the building surface. As in the previous section, the structured Cartesian grid inevitably has a very large side ratio in the belt-like area at the center of the computational domain. Conversely, the HEX grid is well distributed over the whole domain but remains orthogonal. Figure 4d illustrates the *x-z* plane of the grid system utilized for the simulations.

The boundary conditions are as follows. The inflow turbulence generated in the numerical wind tunnel is imposed at the inlet boundary, and a convective boundary condition is imposed at the outlet boundary. A symmetric boundary condition is applied to the lateral and top boundaries. A no-slip boundary condition is imposed on the cylinder surface and at the bottom of the computational domain. A zero-pressure gradient boundary condition is applied at the inlet surface and on the cylinder surface while a zero-pressure condition is applied at the outlet boundary. The simulation starts from rest. The flow field is analyzed after flow statistics become stable.

4.3. Results and discussions

Figure 10 compares wind pressure distributions around a high-rise building at three heights, $h = 5$ m, 41.5 m and 80.3 m, obtained by numerical simulation, with experimental data. The building's height is 84 meters. The X coordinate in Figure 10 denotes one circle around a square cylinder, where the windward side, two crosswind sides, and the leeward side are marked as 3, 2, 4 and 1. When the grid number is 7.2 million, the numerical results obtained for the three grid systems show good agreement with the experimental data. However, with decrease in grid number, deviations among grid systems and experimental data become obvious. The structured Cartesian grid produces negative pressures stronger than the experiment at the side surfaces at the three heights when the grid number is 1.8 million, indicating that the behavior of the separated shear layer is not well resolved. The results produced by the unstructured triangular prism grid are the worst. They deviate from the experimental data at the side surfaces at the three heights when the grid number is 1.8 million and 3.0 million. In particular, the unstructured grid produces pressures at the front edges of the building that are too negative. In general, the HEX grid exhibits the closest agreement with the experimental data at the three heights for the three grid numbers.

One important factor in simulating the flow around a high-rise building immersed in an atmospheric boundary layer is the necessity of generating and maintaining the inflow turbulence. Both of the HEX and the regular Cartesian grids are orthogonal, but the HEX grid obviously has better grid quality. The aspect ratio of the regular Cartesian grid in front of the high-rise building is too high, which may influence the inflow turbulence characteristics. In addition, during the simulation, it is noted that the unstructured triangular prism grid tends to cause numerical oscillation when the grid number is not sufficient, although with the same grid number and the same finest grid size, the other two grid systems do not have this problem. Although such numerical oscillations can be mitigated by reducing the time step of the calculation, the calculation cost is increased.

Figure 11 compares the three-dimensional instantaneous

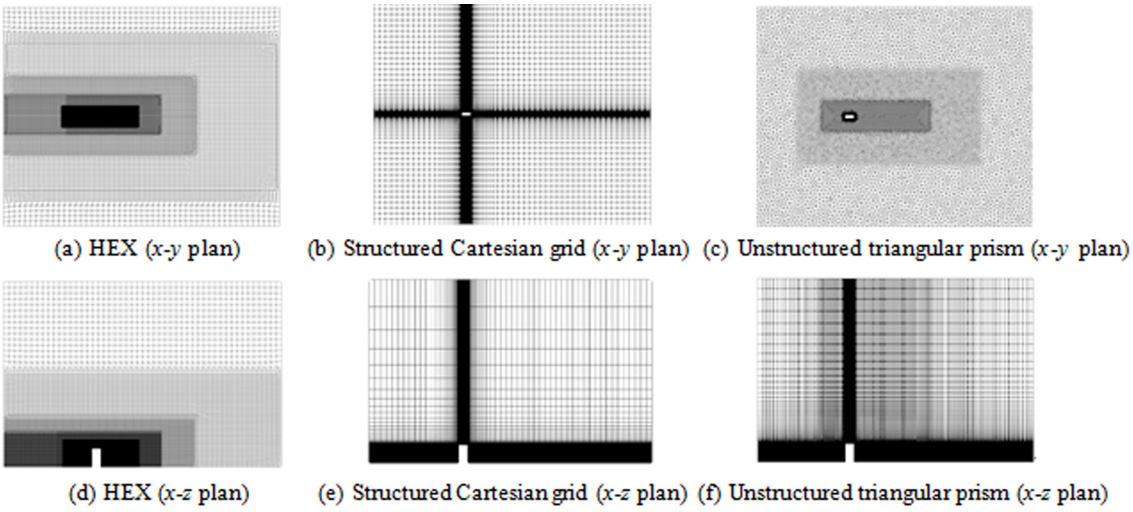


Figure 9. Examples of grid system. (grid number 1.8 million)

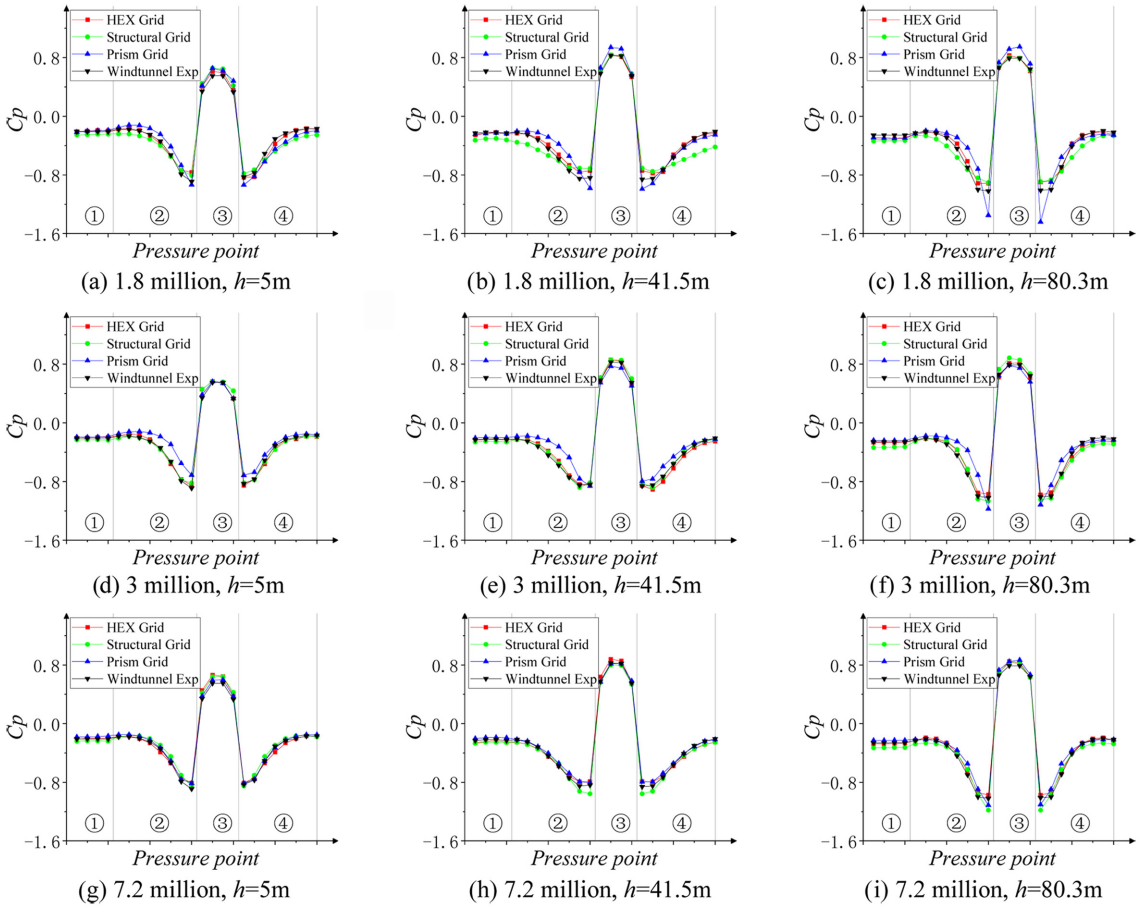


Figure 10. Mean pressure coefficients at three heights

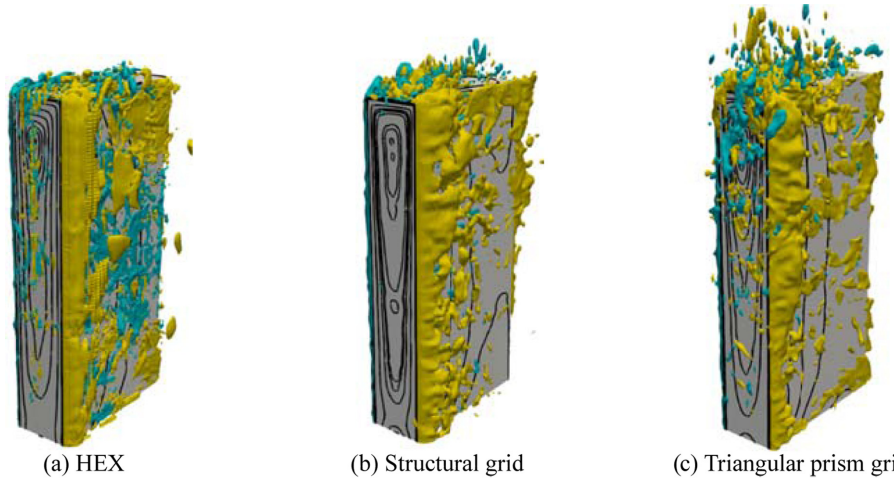


Figure 11. Comparison of instantaneous vortex field obtained by three grid systems. (*blue* $\omega_z^* = -32$, *yellow* $\omega_z^* = +32$)

vorticity field obtained by three grids at the grid number of 7.2 million by illustrating the iso-vorticity surface. The vorticity components are normalized using the free-stream velocity ($\omega^* = \omega d / U_\infty$). All figures show flow separation caused bythe upwind building corner, which results in negative pressures on the side surfaces. Flow separation also occurs at the front roof edge. However, the structured Cartesian grid and the unstructured triangular prism exhibit numerical oscillations when resolving the separated shear flow on the roof.

5. Conclusions

This paper has described large eddy simulations carried

out to simulate wind pressures on a square cylinder in uniform flow and on a high-rise building in boundary layer flow, to investigate the applicability of the HEX grid to simulation in urban areas. Three grid systems were compared for three grid numbers. This study shows that the HEX mesh generally produces the best simulation results for high-rise buildings due to its unique, good-quality grid system. The results demonstrate that the auto hexahedral non-structured mesh has good potential applicability to simulation of urban flows.

As a preliminary study, this paper has presented simulation results with respect to wind that blows directly again a building. In order to clarify the performance of the HEX grid, more simulations considering different wind directions should be carried out.

Acknowledgement

The authors wish to acknowledge the financial support from Key Lab Grant No. SLDRCE19-A-01, National Natural Science Foundation of China Grant No. 51878503 and Cooperative Research Program of Civil Engineering College of Tongji University No. TMGFXK-2018-007.

References

AIJ (2015). Recommendations for loads on buildings. Tokyo, Wind Engineering Center.

Blocken, B. (2013). CFD simulation of pedestrian-level wind conditions around buildings: Past achievements and prospects. *J. Wind Eng. Ind. Aerodyn*., 121, 138-145.

Bearman, P. W. & Obasaju, E. D. (1982). An experimental study of pressure fluctuations on fixed and oscillating square-section cylinders. *Journal of Fluid Mechanics*, 119, 297.

Cao, Y. and Tamura, T. (2016). Large-eddy simulations of flow past a square cylinder using structured and unstructured grids. *Computers & Fluids*, 137, 36-54.

Cheng, C.M., Lu, P..C, Chen, R.H. (1992). Wind loads on square cylinder in homogeneous turbulent flows. *Journal of Wind Engineering*. 41, 739-749.

Durao, G., Heitor, V, Pereira, F. (1988). Measurements of turbulent and periodic flows around a square cross-section cylinder. *Experiments in Fluids*, 6(5), 298-304.

Frohlich, J. et al. (1998). Large eddy simulation of flow around circular cylinders on structured and unstructured Grids. *Notes on Numerical Fluid Mechanics*, 66, 319-338.

Huang, S., Li, Q. S., Xu, S. (2008). Numerical evaluation of wind effects on a tall steel building by CFD. *Steel Construction*, 63(5), 612-627.

Irwin, P. (1981). The design of spires for wind simulation. *Journal of Wind Engineering and Industrial Aerodynamics*, 7, 361-366.

Lee, B.E. (2006). The effect of turbulence on the surface pressure field of a square prism. *Journal of Fluid Mechanics*, 69(2), 263-282.

Lubcke, H., Schmidt, S., Rung, T. (2001). Comparison of LES and RANS in bluff-body flows. *Journal of Wind Engineering & Industrial Aerodynamics*, 89(14), 1471-1485.

Lyn, D.A., Einav, S., Rodi, W. (2006). A laser Doppler velocimetry study of ensemble-averaged characteristics of the turbulent near wake of a square cylinder. *Journal of Fluid Mechanics*, 304, 285-319.

McLean, I., Gartshore, I. (1992). Spanwise correlation of pressure on a rigid square section cylinder. *Journal of Wind Engineering*. 41, 779-808.

Nishimura, H., Taniike, Y. (2000). Fluctuating pressures on a two-dimensional square prism. *Journal of Structural and Construction Engineering*, 533, 37-43. (in Japanese).

Noda, S. (2016). Evaluation of wind force acting on a high-rising building by LES and simulation of wind-excited response. Tokyo Institute of Technology.

Norberg, C. (1993). Flow around rectangular cylinders: Pressure forces and wake frequencies. *Journal of Wind Engineering & Industrial Aerodynamics*, 49(1-3), 187-196.

Nozu, T., Tamura, T., Okuda, Y., Sanada, S. (2008). LES of the flow and building wall pressures in the center of tokyo. *Journal of Wind Engineering and Industrial Aerodynamics*, 96, 1762-1773.

Ohno, O. and Tamura, T. "Unsteady numerical simulation of turbulent flow at the area with high-rise buildings" (in Japanese). Proc. the annual meeting of AIJ, Tokyo, Japan, August, 2001, 99.

Phillips, D.A and Soligo, M.J. (2019). Will CFD ever replace wind tunnels for building wind simulations?. *International Journal of High-Rise Buildings*. 8(2), 107-116.

Srinivas, Y., Biswas, G., Parihar, A.S. (2006). Large-eddy simulation of high Reynolds number turbulent flow past a square cylinder. *Journal of Engineering Mechanics*. 132(3), 327-335.

Tamura, T., Kono, T., Cao, S., Tsubokura Y., Okuda, Y., and Okada, H. (2003) "Numerical analysis of wind loads on tall buildings in urban area". Proc. the CIB-CTBUH Conference on Tall Buildings, Malaysia, 531-538.

Uemura, K. and Saito, T. (1993). Automatic mesh generation for FEM simulation of wind flow around tall buildings. *Journal of Wind Engineering and Industrial Aerodynamics*, 46-47, 357-362.

Weatherill, N.P. (1990). Mixed structured-unstructured meshes for aerodynamic flow simulation. *Aeronautical Journal*, 94, 934.